Synthesis and characterizations of nickel doped Co-Zn-Y ferrites

H. T. Ali[a], N. Amin[b], M. Akhtar[b], M. I. Arshad[b,*], M. K. Athar[b], N. A. Morley[c], M. Yusaf[d], Z. Latif[b], K. Mehmood[b]

[a]*Department of Mechanical Engineering, College of Engineering, Taif University, Taif 21944, Saudi Arabia*

[b]*Department of Physics, Government College University, Faisalabad, Pakistan 38000*

[c]*Department of Materials Science and Engineering, The University of Sheffield, UK, S1 3JD*

[d]*Department of Clinical Pharmacy, College of Pharmacy, Taif University, Taif 21944, Saudi Arabia*

The Nickel substituted Cu-Co-Zn-Ce nano ferrites, $Zn_{0.15}Co_{0.45}Cu_{0.40-x}Ni_x$ $Fe_{1.85}Ce_{0.15}O_4$ with x=0, 0.1, 0.20, 0.30, 0.40, were synthesized using the coprecipitation technique. The sample were sintered at 900 ℃ for 5h. The structural, electrical, dielectric and magnetic properties of all the prepared samples were characterized by XRD, SMU2401, UV-Vis and FTIR. The powder X-ray diffraction patterns of all the prepared samples confirmed the formation of single-phase cubic spinel structures. These samples further characterized for the electrical properties by using two-probe type method. The DC resistivity of all the ferrite composition decreased as the temperature increased, showing their semiconductor nature. UV-Vis and FTIR confirmed the substitution of nickel in Cu-Co-Zn-Ce ferrites. From UV-Vis it is observed that the optical band gap changes from 3.9 eV to 5.3 eV with addition of Ni. FTIR analysis revealed that a strong variation on tetrahedral absorption frequency band is present which is due to the replacement of Ni on Cu. All these results suggested that these materials can be used for wastewater treatment.

(Received October 23, 2022; Accepted January 16, 2023)

Keywords: Co-precipitation, Crystalline size, Bandgap, Resistivity

1. Introduction

In the modern era, ferrites are emerging in high frequency applications. By nature, they attract magnets and iron composed materials. They have many advantages in comparison to other types of magnetic materials e.g. high electrical resistivity and low eddy current losses. Spinel ferrites have FCC structure and formula can be represented as MFe_2O_4. There is occurrence of two kinds of interstitials positions within these lattices and they are engaged by metal cations. Each unit cell contains 96 interstitial sites from which 64 tetrahedral (A) and 32 octahedral (B) sites. At high frequencies, because of their soft magnetic properties and high electrical resistivity spinal ferrites can be used in multilayer chip-inductors and surface mount devices [1, 2]. Much work has been done by doping cerium in soft ferrites but no specific work is done on cerium doped Cu-Co-Zn-Ce nano ferrites, $Zn_{0.15}Co_{0.45}Cu_{0.40-x}Ni_x$ $Fe_{1.85}Ce_{0.15}O_4$ with x=0, 0.1, 0.20, 0.30, 0.40 ferrites. Cu-Ni-Zn-Co -Ce ferrites have no inherent toxicity and this material is synthesized by Co-precipitation technique which is commonly used for making stoichiometric calculations to form homogeneous nanoparticles [3-4]. The optical and structural properties depend upon the kind of positive ions and their distribution between octahedral and tetrahedral sites [4-5]. To improve their physical characteristics, the synthesized ferrites were formed by different methods including sol-gel [6], co-precipitation [7], hydrothermal [8], auto combustion [9], electrochemical [10], precursor [11] and micro-emulsion methods [12]. The chemical co-precipitation method is a largely preferable method due to its simplicity and good control on the crystalline size for synthesized nanoparticles

* Corresponding author: mimranarshad@gcuf.edu.pk
https://doi.org/10.15251/JOR.2023.191.65

in addition to other properties of materials. This chemical method is to prepared nanoparticles in a larger amount in a relatively short interval of time. The chemical co-precipitation is the best suitable, inexpensive, simplest,, and easiest method [13 -15].

In this research work, Nickel substituted Cu-Co-Zn-Ce nano ferrites, $Zn_{0.15}Co_{0.45}Cu_{0.40-x}Ni_x$ $Fe_{1.85}Ce_{0.15}O_4$ with x=0, 0.1, 0.20, 0.30, 0.40, (***Ni doped CCZC-ferrite***) were synthesized by employing co-precipitation method. In this study we investigate the structural, optical and electrical properties of nickel doped CCZC-ferrites with addition of nickel.

2. Materials and methods

The Ni doped CCZC-ferrite were synthesized by co-precipitation technique. By making stoichiometric calculation the raw material used for the fabrication of nanoparticles were Cobalt Nitrate hexahydrate ($Co(NO_3)_2.6H_2O$), Iron Chloride Hexahydrate. ($Fe(NO_3)_3.9H_2O$), Cerium Nitrate hexahydrate ($Ce(NO_3)_3.6H_2O$), Zinc Nitrate ($Zn(NO_3)_2$), Copper Nitrate ($Co(NO_3)_2$) and Nickel Nitrate ($Ni(NO_3)_2$). These precursors were dissolved in 100 ml water and then stirred the solution to make a homogeneous mixture by magnetic stirring for 50 minutes and 0.35 mole NaOH is mixed in the solution to maintain the pH 7. After stirring the solution is put in the water bath for overnight then the material was washed with ethanol three to four times to remove the impurities. To dry the samples all the samples were put into oven for 24 hours at 80 ℃. After that the materials were sintered at 900 ℃ for 5 hr and grinded. These samples were characterized by characterized by XRD (X-ray diffract meter), FTIR (Fourier Transmission electron microscope), IV Two probe characterization technique.

3. Result and discussion

3.1. X-Ray Diffraction Analysis

Crystalline Structure and formation of spinel structure has been investigated by XRD. Figures Showed the XRD pattern of synthesized nanoparticles that contain Ni doped CCZC-ferrite which synthesized by coprecipitation method. The different peaks with planes (220),(311),(400),(511) confirms the formation of single phase spinel ferrite. The X-ray diffraction peak (311) was used to calculate the crystallite size using the Debye–Scherrer Equation [16].

$$D = \frac{0.9\lambda}{\beta \cos\theta} \quad (1)$$

Where D represents crystallite size, λ is the wavelength of X-rays and its value is 1.542Å and β is full width at half maximum of XRD peaks. All diffraction peaks representing advanced degree of crystallinity with well-defined peaks. The crystallite size was varied with the insertion of Ni in CCZC-ferrite (as shown in Fig. 2). It may be due to the incorporation of Ni in ferrite lattice. The lattice constant (a) was estimated using equation [17, 18];

$$a_{exp} = d\sqrt{h^2 + k^2 + l^2} \quad (2)$$

Here, $h\ k\ l$ is the miller indices of the planes. The interplanar distance (d) is to be determined by using the Braggs equation that is given below [19,20];

$$2dsin\theta = n\lambda \quad (3)$$

where n is the order of reflection. The volume of the unit cell (V) was estimated *via* the below equation [21];

$$V_{cell} = a^3 \quad (4)$$

The lattice constant, interplanar distance, and unit cell volume were reduced with increasing the Ni percentage. The increase in lattice parameters may be due to the incorporation of Ni in CCZC-ferrite.

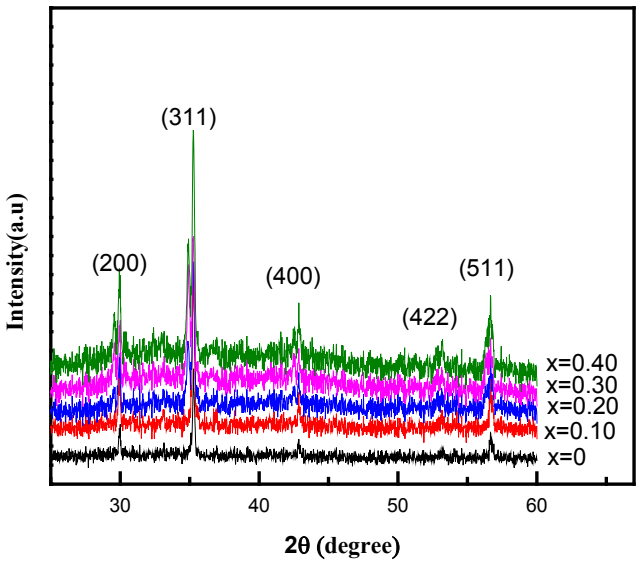

Fig. 1. Combined XRD pattern of Ni doped CCZC-ferrite

For the higher concentration of Nickel x=0.2, 0.40, the increasing trend in the lattice parameter may be owed to variations in cationic distributions. Similar results have been reported by other researchers [19, 20]. The theoretical values of all the fabricated compositions were calculated using relation (5) [21].

$$a_{th} = \frac{8}{3\sqrt{3}}\left[(r_A + R_0) + \sqrt{3}(r_B + R_0)\right] \tag{5}$$

where r_A represents ionic radius at tetrahedral A-site, r_B represents the ionic radius at octahedral B-site and R_0 is known as an oxygen ion radius (1.32Å).

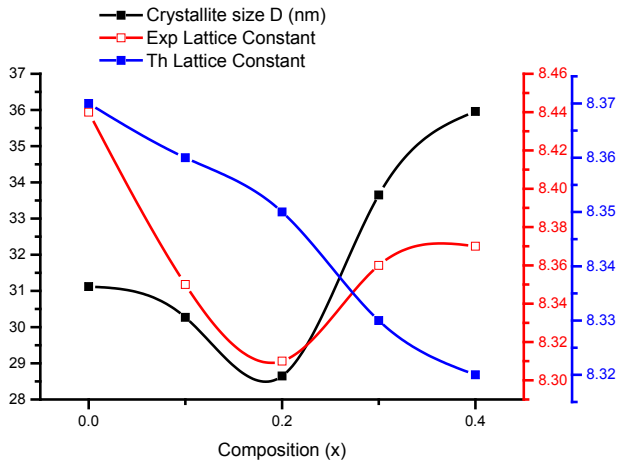

Fig. 2 . Crystallite size and Lattice constants (a_{exp}, a_{th}) as a function of concentration of Ni of Ni doped CCZC-ferrite

X-ray density was evaluated using the equations (6) [22] and values were given in table 1.

$$d_x = \frac{8M}{NV} \tag{6}$$

where M represents the molecular weight of the synthesized compositions, N is the Avogadro's number (6.0221×1023 g/mol-1), V stands for unit cell volume [23]. Table 1 shows the variations of X-ray density with the increasing concentration of Nickel content x=0.0-0.40. Several other parameters like specific surface area (S), packing factor (p) and strain (ε) were calculated using equations (7) to (9) [24], and listed in Table 1.

$$S = \frac{6000}{\rho_x D} \tag{7}$$

$$p = \frac{D}{d} \tag{8}$$

$$\varepsilon = \frac{1}{d^2} \tag{9}$$

Table 1. *XRD parameters of* Ni doped CCZC-ferrite.

Composition (x)	**2θ**	**hkl**	**X-Ray Density**	**Volume of unit cell (Å^3)**	**Packing Factor**	**Strain**	**Specific Surface Area**
0	35.28	311	4.46	598.53	28.01	0.153	24.67
0.15	35.95	311	4.57	594.64	38.68	0.156	34.85
0.30	35.41	311	4.53	585.67	32.16	0.159	45.79
0.45	35.51	311	4.52	580.15	38.34	0.157	37.46
0.60	35.86	311	4.41	573.15	43.06	0.155	34.59

3.2. UV–visible spectroscopy

The optical band gap energy was obtained from UV-Vis plots of the synthesized Ni doped CCZC-ferrites. All the samples were dissolved in deionized water to do the UV-Vis spectroscopy. The absorption coefficient of fabricated material was found using the following relation (10) [25].

$$\alpha = \frac{2.303 \log(A)}{t} \tag{10}$$

where, A stands for optical absorbance, while t represents pallet thickness. The bandgap energy and absorption coefficient are associated with the following relation (11) [26] as.

$$\alpha h\nu = B\left(h\nu - E_g\right)^m \tag{11}$$

Here, B is a constant term, $h\nu$ is the incident photon energy. the constant m is dependent on the nature of the transition between valence and conduction band, for direct bandgap materials m is taken to be ½ while for indirect bandgap materials m takes the value 2. Fig. 3 shows the bandgap energy vs Ni concentration.

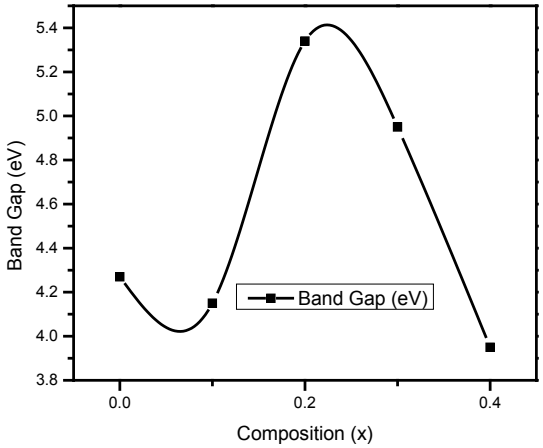

Fig. 3. Pattern of Bandgap energy (eV) of Ni doped CCZC-ferrite.

3.3. Current Voltage Analysis

The current voltage (I-V) characteristics were done by SMU 2401 of Ni doped CCZC-ferrite. To obtain the DC resistivity following relation is used [27,28].

$$\rho = \frac{RA}{L} \tag{12}$$

Here R was found by relation R= 1/slope of I-V graph, Where A represents the area of pellets and L represents the thickness of the pellet. The resistivity increases with an increase in temperature up to a specific temperature after that, the resistivity starts decreasing with a further increase in temperature. This transition point is called curie temperature. The curie temperature lies between 323K and 353K. The relation between resistivity and temperature is given by Equation (13) [29].

$$\rho = \rho_o exp\left(\frac{\Delta E}{K_B T}\right) \tag{13}$$

where ρ is electrical resistivity, $\rho_o$is the resistivity at infinite temperature, ΔE is activation energy and K_B is Boltzmann's constant.

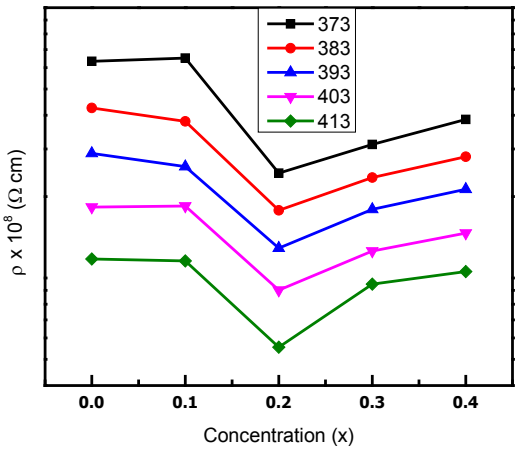

Fig. 4. Graph of ρ vs. Ni concentration of Ni doped CCZC-ferrite.

The activation energy was determined using equation (13). It is also evident from fig. 5 that activation energy for the paramagnetic region is greater than the activation energy for the ferrimagnetic region. This may be ascribed to the ordered magnetic domains in the ferrimagnetic region while randomly oriented magnetic domains in the paramagnetic region so more energy are required for the ions to jump from one cation to another [30].

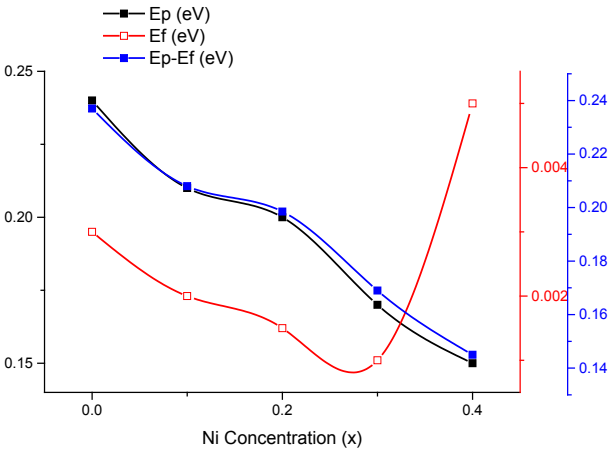

Fig. 5. Graph of activation energy of ferrimagnetic region (E_f) and paramagnetic region (E_P) with concentration (x) of Ni doped CCZC-ferrite.

3.4. FTIR analysis

FTIR analysis was performed for investigating the chemical functional groups of synthesized nano ferrites of Ni doped CCZC-ferrite. The lower frequency absorption band (V_2) exhibited in the range of 417 cm^{-1} to 422 cm^{-1} while the upper-frequency absorption band (V_1) is in the range of 560 cm^{-1} to 690 cm^{-1}, the values of V_1 and V_2 and their relative intensities are given in Fig. 6. A slight variation in V_2 is observed but V_1 has great variations in Ni doped CCZC-ferrite. it has been reported that band which was observed in the high-frequency region is related to the tetrahedral site (A-site), while the band detected in low-frequency region is connected to the octahedral site (B-site) [26-29]. The high-frequency band observed from 560 cm^{-1} to 690 cm^{-1} may be ascribed to stretching vibrations of tetrahedral site metal-oxygen bonding, which confirms the replacement of Cu with Ni. The tetrahedral site stretching vibrations first shifted to higher values from x=0 to x=0.20 and then decreased for the concentration x=0.40.

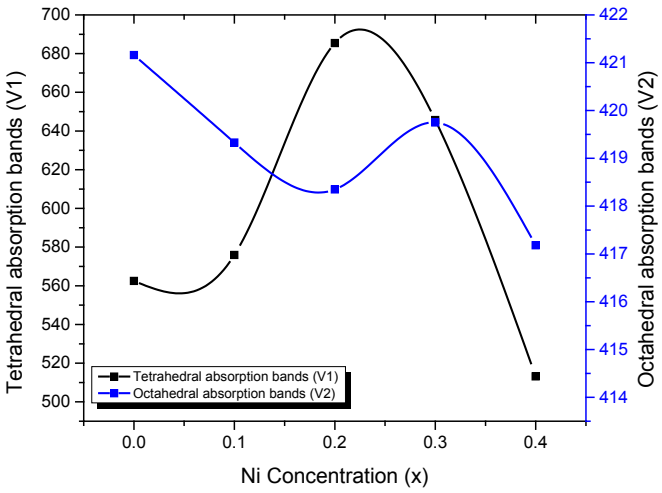

Fig. 6. Variation Frequency absorption bands (V_1 and V_2) with Ni of Nickel doped CCZC-ferrites.

4. Conclusion

Co-precipitation technique was employed for the fabrication of Ni^{2+} doped spinel soft ferrites with chemical composition $Zn_{0.15}Co_{0.45}Cu_{0.40-x}Ni_x\ Fe_{1.85}Ce_{0.15}O_4$ with x=0, 0.1, 0.20, 0.30, 0.40 nanoparticles annealed at 1173 K for 5 hours. XRD patterns exhibited the formation of the cubic spinel structure of the synthesized specimen. The crystallite size and lattice parameter have a decreasing trend with the inclusion of Ni^{2+} content from x=0 to x=0.20, then an increasing trend was found with the further increase on Ni^{2+} up to x=0.40. The DC resistivity decreased from x= 0 to x=0.20 after that the resistivity increased up to x=0.40. The bandgap energy increased from x=0 to x=0.20 after that its decreased upto x= 0.40. The activation energy decreased with increase of Ni concentration. A strong variation on tetrahedral absorption band confirmed the substitution of Ni on tetra site. All these results revealed that these materials may be utilized for waste water treatment.

References

[1] S.-F. Wang, Y.-F. Hsu, K.-M. Chou, J.-T. J. J. o. M. Tsai, and M. Materials, "Effects of co-dopants on the magnetic properties of Ni-Zn ferrites," vol. 374, pp. 402-410, 2015; https://doi.org/10.1016/j.jmmm.2014.08.075

[2] Z. Liu, Z. Peng, and X. J. C. I. Fu, "Structural and electromagnetic properties of Ni0. 5Zn0. 5HoxFe2-xO4 ferrites," vol. 43, no. 17, pp. 14938-14944, 2017; https://doi.org/10.1016/j.ceramint.2017.08.011

[3] M. Houshiar and L. J. M. R. B. Jamilpanah, "Effect of Cu dopant on the structural, magnetic and electrical properties of Ni-Zn ferrites," vol. 98, pp. 213-218, 2018; https://doi.org/10.1016/j.materresbull.2017.10.024

[4] M. Sutar and A. J. M. T. P. Patil, "Magnetic Characterization and Instrumentation Setup for Measurement of Co-efficient of Magnetostriction on Co0. 9Ni0. 1Fe2-xMnxO4 Ferrite," vol. 2, no. 4-5, pp. 1494-1501, 2015; https://doi.org/10.1016/j.matpr.2015.07.075

[5] W. Small IV, P. Singhal, T. S. Wilson, and D. J. J. J. o. m. c. Maitland, "Biomedical applications of thermally activated shape memory polymers," vol. 20, no. 17, pp. 3356-3366, 2010; https://doi.org/10.1039/b923717h

[6] E. Oumezzine, S. Hcini, M. Baazaoui, E.-K. Hlil, and M. J. P. T. Oumezzine, "Structural, magnetic and magnetocaloric properties of Zn0. 6− xNixCu0. 4Fe2O4 ferrite nanoparticles prepared by Pechini sol-gel method," vol. 278, pp. 189-195, 2015; https://doi.org/10.1016/j.powtec.2015.03.022

[7] A. S. Albuquerque, J. D. Ardisson, W. A. Macedo, and M. C. J. J. o. A. P. Alves, "Nanosized powders of NiZn ferrite: synthesis, structure, and magnetism," vol. 87, no. 9, pp. 4352-4357, 2000; https://doi.org/10.1063/1.373077

[8] D. Makovec, M. Drofenik, and A. J. J. o. t. A. C. S. Žnidaršič, "Hydrothermal synthesis of manganese zinc ferrite powders from oxides," vol. 82, no. 5, pp. 1113-1120, 1999; https://doi.org/10.1111/j.1151-2916.1999.tb01884.x

[9] R. K. Selvan, C. Augustin, L. J. Berchmans, and R. J. M. R. B. Saraswathi, "Combustion synthesis of CuFe2O4," vol. 38, no. 1, pp. 41-54, 2003; https://doi.org/10.1016/S0025-5408(02)01004-8

[10] G. Goya, H. Rechenberg, and J. J. J. o. a. p. Jiang, "Structural and magnetic properties of ball milled copper ferrite," vol. 84, no. 2, pp. 1101-1108, 1998; https://doi.org/10.1063/1.368109

[11] F. Li, J. Liu, D. G. Evans, and X. J. C. o. m. Duan, "Stoichiometric synthesis of pure MFe2O4 (M= Mg, Co, and Ni) spinel ferrites from tailored layered double hydroxide (hydrotalcite-like) precursors," vol. 16, no. 8, pp. 1597-1602, 2004; https://doi.org/10.1021/cm035248c

[12] C. T. Seip, E. E. Carpenter, C. J. O'Connor, V. T. John, and S. J. I. t. o. m. Li, "Magnetic properties of a series of ferrite nanoparticles synthesized in reverse micelles," vol. 34, no. 4, pp.

1111-1113, 1998; https://doi.org/10.1109/20.706388

[13] S. Hcini, A. Omri, M. Boudard, M. L. Bouazizi, A. Dhahri, and K. J. J. o. M. S. M. i. E. Touileb, "Microstructural, magnetic and electrical properties of Zn 0.4 M 0.3 Co 0.3 Fe 2 O 4 (M= Ni and Cu) ferrites synthesized by sol-gel method," vol. 29, no. 8, pp. 6879-6891, 2018; https://doi.org/10.1007/s10854-018-8674-3

[14] A. Farea, S. Kumar, K. M. Batoo, A. Yousef, C. G. J. J. o. A. Lee, and Compounds, "Structure and electrical properties of Co0. 5CdxFe2. 5− xO4 ferrites," vol. 464, no. 1-2, pp. 361-369, 2008; bhttps://doi.org/10.1016/j.jallcom.2007.09.126

[15] M. Hasan et al., "Mg and La co-doped ZnNi spinel ferrites for low resistive applications," vol. 6, no. 1, p. 016302, 2018; https://doi.org/10.1088/2053-1591/aae3f6

[16] N. Amin et al., "Impacts of substituting Ni 2 ions on structural and electrical properties of W-type Barium Based Hexaferrites," vol. 14, no. 2, pp. 501-507, 2019.

[17] K. Hussain, A. Bibi, F. Jabeen, N. Amin, K. Mahmood, A. Ali, M.Z. Iqbal, M.I. Arshad, Study of structural, optical, electrical and magnetic properties of Cu2+doped Zn0.4Co0.6-xCe0.1Fe1.9O4 spinel ferrites, Phys. B Condens. Matter. 584(1), 412078 (2020); https://doi.org/10.1016/j.physb.2020.412078

[18] K. Hussain et al., "Investigation of structural and electrical properties of Ce3+ ions substituted Cd-Co ferrites," vol. 14, no. 1, pp. 85-92, 2019.

[19] N. Amin et al., "Structural, electrical, optical and dielectric properties of yttrium substituted cadmium ferrites prepared by Co-Precipitation method," 2020; https://doi.org/10.1016/j.ceramint.2020.05.079

[20] A. Aslam, A.U. Rehman, N. Amin, M. Ajaz un Nabi, Q. ul ain Abdullah, N.A. Morley, M.I. Arshad, H.T. Ali, M. Yusuf, Z. Latif, K. Mehmood, J. Phys. Chem. Solids. 154 110080 (2021); https://doi.org/10.1016/j.jpcs.2021.110080

[21] A.U. Rehman, N. Morley, N. Amin, M.I. Arshad, M.A. un Nabi, K. Mahmood, A. Ali, A. Aslam, A. Bibi, M.Z. Iqbal, Ceramics International, 46 (2020) 29297-29308; https://doi.org/10.1016/j.ceramint.2020.08.106

[22] K. Hussain, N. Amin, M.I. Arshad, Ceramics International, 47 (2021) 3401-3410; https://doi.org/10.1016/j.ceramint.2020.09.185

[23] A. Aslam, A. Razzaq, S. Naz, N. Amin, M.I. Arshad, M. Nabi, A. Nawaz, K. Mahmood, A. Bibi, F. Iqbal, Journal of Superconductivity and Novel Magnetism, 34 (2021) 1855-1864; https://doi.org/10.1007/s10948-021-05802-4

[24] N. Amin, M. Akhtar, M. Sabir, K. Mahmood, A. ALIa, G. Mustafa, M. Hasan, A. Bibi, M. Iqbal, F. Iqbal, , Journal of Ovonic Research, 16 (2020) 11-19.

[25] I. ALIa, N. Amin, A. Rehman, M. Akhtar, M. Fatima, K. Mahmood, A. ALIa, G. Mustafa, M. Hasan, A. Bibi, Digest Journal of Nanomaterials and Biostructures, 15 (2020) 67-73.

[26] A. Aslam, A.U. Rehman, N. Amin, M. Amami, M. Nabi, H. Alrobei, M. Asghar, N. Morley, M. Akhtar, M.I. Arshad, Journal of Superconductivity and Novel Magnetism, 35 (2022) 473-483; https://doi.org/10.1007/s10948-021-06085-5

[27] N. Amin, A. Razaq, A.U. Rehman, K. Hussain, M. Nabi, N. Morley, M. Amami, A. Bibi, M.I. Arshad, K. Mahmood, Journal of Superconductivity and Novel Magnetism, (2021) 1-11; https://doi.org/10.1007/s10948-021-06053-z

[28] M.I.U. Haq, M. Asghar, M.A.U. Nabi, N. Amin, S. Tahir, M.I. Arshad, Journal of Superconductivity and Novel Magnetism, 35 (2022) 719-732; https://doi.org/10.1007/s10948-021-06124-1

[29] M.I. Arshad, M. Hasan, A.U. Rehman, M. Akhtar, N. Amin, K. Mahmood, A. Ali, T. Trakoolwilaiwan, N.T.K. Thanh, Ceramics International, 48 (2022) 14246-14260; https://doi.org/10.1016/j.ceramint.2022.01.313

[30] G. Abbas, A.U. Rehman, W. Gull, M. Afzaal, N. Amin, L. Ben Farhat, M. Amami, N.A. Morley, M. Akhtar, M.I. Arshad, Journal of Sol-Gel Science and Technology, (2022) 1-15; https://doi.org/10.1007/s10971-021-05713-9